Plasma Science and Technology

PAPER

# Automated electron temperature fitting of Langmuir probe *I–V* trace in plasmas with multiple Maxwellian EEDFs

To cite this article: Chi-Shung YIP *et al* 2020 *Plasma Sci. Technol.* **22** 085404

 

Plasma Sci. Technol. **22** (2020) 085404 (11pp) https://doi.org/10.1088/2058-6272/ab7f3d

# Automated electron temperature fitting of Langmuir probe *I–V* trace in plasmas with multiple Maxwellian EEDFs

**Chi-Shung YIP (叶孜崇)[1], Wei ZHANG (张炜)[1], Guosheng XU (徐国盛)[1] and Noah HERSHKOWITZ[2]**

[1] Institute of Plasma Physics, Chinese Academy of Sciences, Hefei 230031, People's Republic of China
[2] Department of Engineering Physics, University of Wisconsin—Madison, Madison, WI 53706, United States of America

E-mail: zhangwei@ipp.ac.cn

Received 20 November 2019, revised 9 March 2020
Accepted for publication 11 March 2020
Published 12 June 2020

**Abstract**

An algorithm for automated fitting of the effective electron temperature from a planar Langmuir probe *I–V* trace taken in a plasma with multiple Maxwellian electron populations is developed through MATLAB coding. The code automatically finds a fitting range suitable for analyzing the temperatures of each of the electron populations. The algorithm is used to analyze *I–V* traces from both the Institute of Plasma Physics Chinese Academy of Sciences's Diagnostic Test Source device and a similar multi-dipole chamber at the University of Wisconsin–Madison. *I–V* traces reconstructed from the parameters fitted by the algorithm not only agree with the measured *I–V* trace but also reveal physical properties consistent with those found in previous studies. Cylindrical probe traces are also analyzed with the algorithm and it is shown that the major source of error in such attempts is the disruption of the inflection point due to both decreased signal-to-noise ratio and greater sheath expansion. It is thus recommended to use planar probes with radii much greater than the plasma Debye length when signal-to-noise ratio is poor.

Keywords: EEDF, Langmuir probes, plasma diagnostics

(Some figures may appear in colour only in the online journal)

## 1. Introduction

Since their introduction by Irving Langmuir [1], Langmuir probes are arguably the most important plasma diagnostic. They are widely used in fusion research [2, 3] and in low temperature plasmas [4–8]. They provide a simple, robust, cost effective, and relatively accurate way to measure key parameters including the electron temperature $T_e$, electron density $n_e$, and sometimes the plasma potential $V_p$. As measurements are performed through directly collecting electrons of selected energies, Langmuir probe measurements do not require the assumption of the electron energy distribution functions (EEDFs) being single Maxwellian. The assumption of the diagnosed plasma having a single Maxwellian EEDF is often required by cutoff frequency measurements and optical diagnostics [9] which do not return an electron energy spectrum. Because a Langmuir probe directly measures the EEDF through selective absorption of electrons with the probe's bias, it also has the almost unique advantage of diagnosing plasmas with complex EEDFs like double Maxwellian and triple Maxwellian distributions [10] as well as plasmas with electron and ion beams.

Arguably the most physically accurate analysis of Langmuir probe *I–V* characteristics is to extract the measured EEDFs through differentiating the *I–V* trace twice [11] (or once when the diagnosed plasma is strongly magnetized [12]). This, however, is often unrealistic for probes in noisy environments as any noise will become amplified when each derivative is calculated. In addition, virtual cathodes near large probes and/or potential distortion by contaminated probe surfaces tend to disrupt the *I–V* traces near the plasma potential [13–15], causing $d^2I/dV^2$ to become distorted. These problems are visually demonstrated in figure 1.

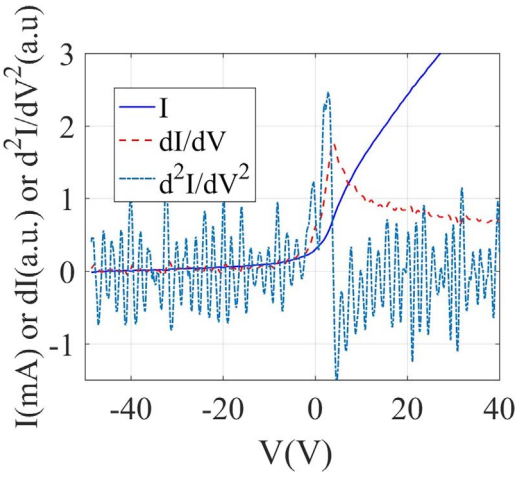


**Figure 1.** $\mathrm{d}I/\mathrm{d}V$ and $\mathrm{d}^2I/\mathrm{d}V^2$ of a noisy Langmuir probe trace. The high frequency noise is amplified with each derivative.

An alternative procedure is to fit the *I–V* characteristics assuming some form of EEDFs. Since information regarding the EEDF is not physically lost in the data acquisition process, one can choose the form of the EEDFs that best fits the *I–V* trace. This is important as most linear devices are known to create at least two species of electrons: a hot species created through electron heating by the plasma source, and a cold species created through ionization of neutral gas. Limited confinement in these devices prevents electrons from totally thermalizing, so electrons created from these different mechanisms remain separate Maxwellian distributions spatially overlapping each other. In these plasmas the ability to fit multiple Maxwellian distributions is thus an important way to understand the EEDFs and the mechanism behind their formation in these devices. Traditionally double Maxwellian and triple Maxwellian EEDFs are fit by manually [16] determining the portion of the *I–V* trace most suitable to fit a straight line with the *I–V* trace drawn on a semi-log graph. This method is adequate if there are only a few Langmuir probe traces per experiment to be analyzed, but becomes very tiresome and prone to human error if, for example, a spatial or temporal distribution of parameters is needed which can require dozens or even hundreds of traces to be analyzed from each experiment [17]. Commercially available Langmuir probes generally come with automated fitting of single Maxwellian EEDFs, but not double Maxwellian EEDFs. This is due to the difficulty in automating the determination of a suitable fitting range of the hotter species of electrons. In this work, we present a procedure to automate single Maxwellian, double Maxwellian and triple Maxwellian fitting of Langmuir probe *I–V* traces with fitting ranges automatically selected through repeated and iterative fitting.

## 2. Experimental setup

The fitting algorithm presented in this work is used to analyze *I–V* traces from the Diagnostics Test Source (DTS) at the Institute of Plasma Physics in Hefei, China, as well as those from the multi-dipole filament discharge device at the University of Wisconsin–Madison, USA, described elsewhere [10].

The DTS multi-dipole confined plasma device consists of a 25 cm diameter, 60 cm long vacuum chamber. Multi-dipole confinement was invented by Limpaecher and Mackenzie and its detailed working principles can be found in [18]. Plasma is produced through impact ionization from primary electrons produced by two 12 cm long, ohmically heated tungsten filaments located near the end wall, emitting the discharge current $I_{\mathrm{Dis}}$. In this experiment we employ argon gas to produce a plasma consisting of positive ions and electrons. 16 rows of permanent magnets surround the radial wall, providing multi-dipole confinement resulting in a uniform plasma [18]. A schematic of the setup is presented in figure 2.

A radially movable Langmuir probe is employed to measure the electron temperature $T_{\mathrm{e}}$, the plasma density $n_{\mathrm{e}}$, and the local potential $V_{\mathrm{p}}$. The movable range of the probe spans the chamber's diameter. The planar Langmuir probe employed in this experiment is constructed with a 0.2 mm thick, 8 mm diameter tantalum disc spot welded onto a 0.8 mm diameter copper plated stainless steel wire, covered by a 2 mm diameter single holed ceramic tube connecting it to the 4 mm diameter stainless steel probe shaft. For the cylindrical probe, a 0.15 mm diameter, 19 mm long tungsten wire is fitted into a 0.8 mm copper tube covered by a single holed ceramic tube connected to an identical shaft. Figure 3 shows a schematic of the probe tips.

## 3. Iterative fitting process

A MATLAB code is developed for the iterative Langmuir probe *I–V* trace fitting process, described below. The flow charts of single Maxwellian, double Maxwellian and triple Maxwellian fittings are illustrated in figures 4–6 respectively. These automated fitting processes were developed from previous ones in which the fitting ranges were determined manually [16], as described below.

The first step of the single Maxwellian fitting process is to fit a straight line to the ion-saturation current $I_{\mathrm{is}}$ data over a 10 V range, beginning with the minimum voltage, as illustrated in figure 7(a). $I_{\mathrm{is}}$ will be subtracted from the *I–V* trace and the $I_{\mathrm{is}}$ subtracted trace will be used for all three fitting processes. The trace is then preliminarily fitted for the electron temperature $T_{\mathrm{e1}}$ in the fitting range of $(V_{\mathrm{inf}} - 1\,\mathrm{V}) < V < V_{\mathrm{inf}}$, where $V_{\mathrm{inf}}$ is the inflection point voltage. The region near $V_{\mathrm{inf}}$, being near the plasma potential $V_{\mathrm{p}}$, corresponds to both the maximum slope and the lowest energy part of the *I–V* trace, i.e., the coldest electron species in the *I–V* trace for a multiple Maxwellian EEDF plasma. In this work, we have chosen an effective electron temperature $T_{\mathrm{eff}} = 1/\Sigma_{\mathrm{s}}(n_{\mathrm{s}}/(n_{\mathrm{e}}T_{\mathrm{s}}))$, where $n_{\mathrm{s}}$ and $T_{\mathrm{s}}$ are the density and temperature of the Maxwellian electron populations. This effective temperature, weighed towards colder electron species, determines the Bohm velocity as well as the ion acoustic speed in a plasma with multiple Maxwellian EEDFs [19, 20]. In addition, $V_{\mathrm{inf}}$ is not taken as the plasma potential $V_{\mathrm{p}}$ *a priori* even when

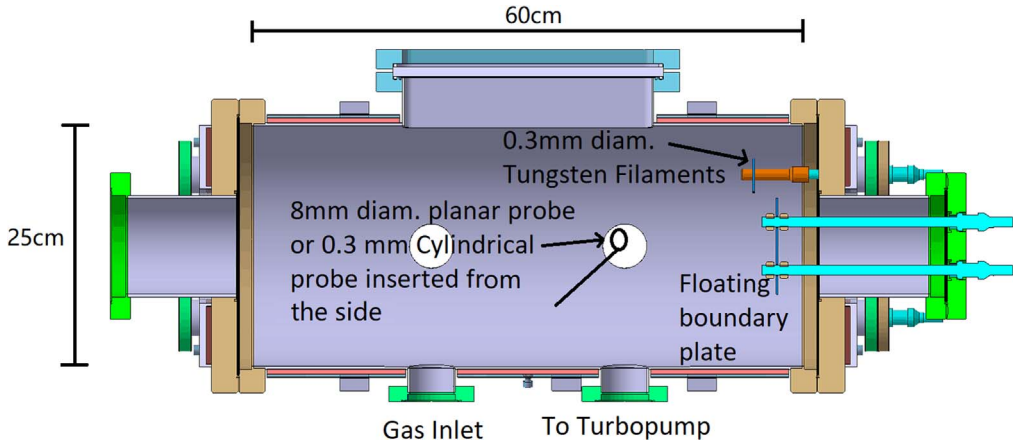


**Figure 2.** Schematic of DTS.

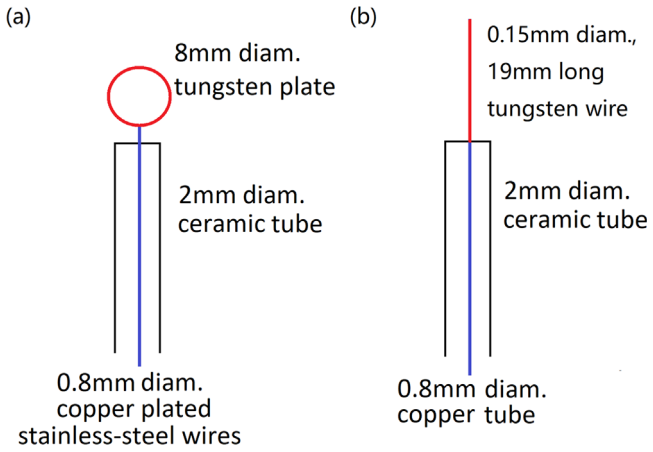


**Figure 3.** Schematics of the (a) planar Langmuir probe, and the (b) cylindrical Langmuir probe.

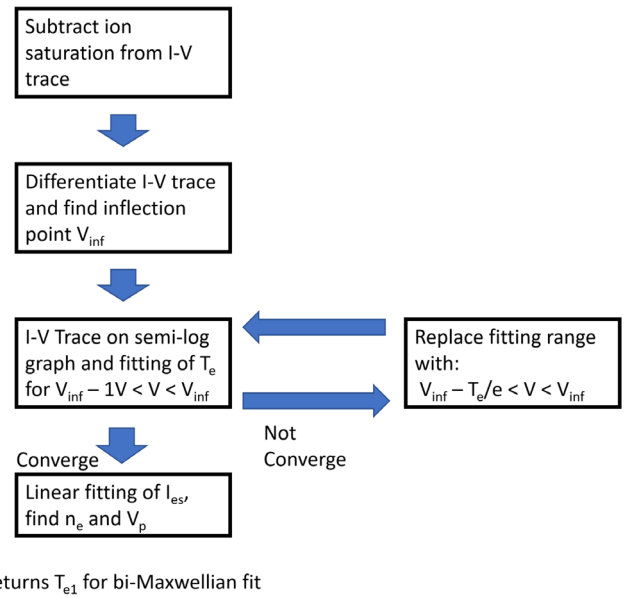


**Figure 4.** Flow chart for the single Maxwellian fitting algorithm.

assuming a non-drifting Maxwellian EEDF, as effects altering $V_{\rm inf}$ including contaminated probe surfaces and the formation of virtual cathodes near $V_{\rm p}$ are not automatically dismissed [13, 15].

The fitting process of $T_{\rm e1}$ is repeated using the resultant $T_{\rm e1}$ to determine the fitting range $(V_{\rm inf} - T_{\rm e1}/e) < V < V_{\rm inf}$ for the next iteration, until $T_{\rm e1}$ converges within 0.05 eV of its previous iteration. This allows the final fitting range for $T_{\rm e1}$ to be determined by the EEDF itself, consistently giving fitting a range of 63% of the lowest energy electrons in the EEDF no matter what $T_{\rm e}$ is, if the EEDF is single Maxwellian. This is because at $T_{\rm e}/e$ below the plasma potential, the probe repels approximately 37% of the electrons according to the Boltzmann relation, thus using the proportion of the $I$–$V$ trace above $V = V_{\rm p} - T_{\rm e}/e$ includes the contribution of 100%–37% = 63% of the electrons from a single Maxwellian EEDF.

Electron saturation is then linearly fitted [21] over the fitting range $(V_{\rm inf} + 5\,{\rm V}) < V < (V_{\rm inf} + 10\,{\rm V})$, and an interception with the exponential fitting of $T_{\rm e1}$ extended beyond $V_{\rm inf}$ is taken as $I_{\rm es}$ and $V_{\rm p}$ assuming a non-drifting EEDF. The 5 V voltage range immediately after $V_{\rm inf}$ is excluded from the fitting range to prevent virtual cathode and surface contamination effects being confused with electron saturation. For simplicity, the change of the probe's effective area due to sheath expansion is approximated to increase linearly with the probe bias, and so does the saturation current. Since this is not always the case [22, 23], choosing a fitting range close to $V_{\rm p}$ can improve accuracy. If a probe is found to be sufficiently cylindrical, i.e. the radius of the probe $r_{\rm probe}$ is much smaller than the Debye length $\lambda_{\rm Debye}$, then the interception method is inappropriate [21]. In that case, $V_{\rm inf}$ will be taken as $V_{\rm p}$ from which the electron saturation current $I_{\rm es}$ and the electron density $n_{\rm e}$ is calculated from the $I$–$V$ trace. This is determined through two criteria: either the resultant $V_{\rm p}$ is smaller than $V_{\rm inf}$, or the resultant $I_{\rm es}$ is smaller than the measured current $I_{\rm inf}$ at the interception point. These criteria are used because virtual cathode and surface contamination effects can reduce the $V_{\rm inf}$ and $I_{\rm es}$ but not increase them [13, 15].

Parameters from the single Maxwellian fitting are then used to fit a double Maxwellian EEDF to the $I$–$V$ trace with $I_{\rm is}$

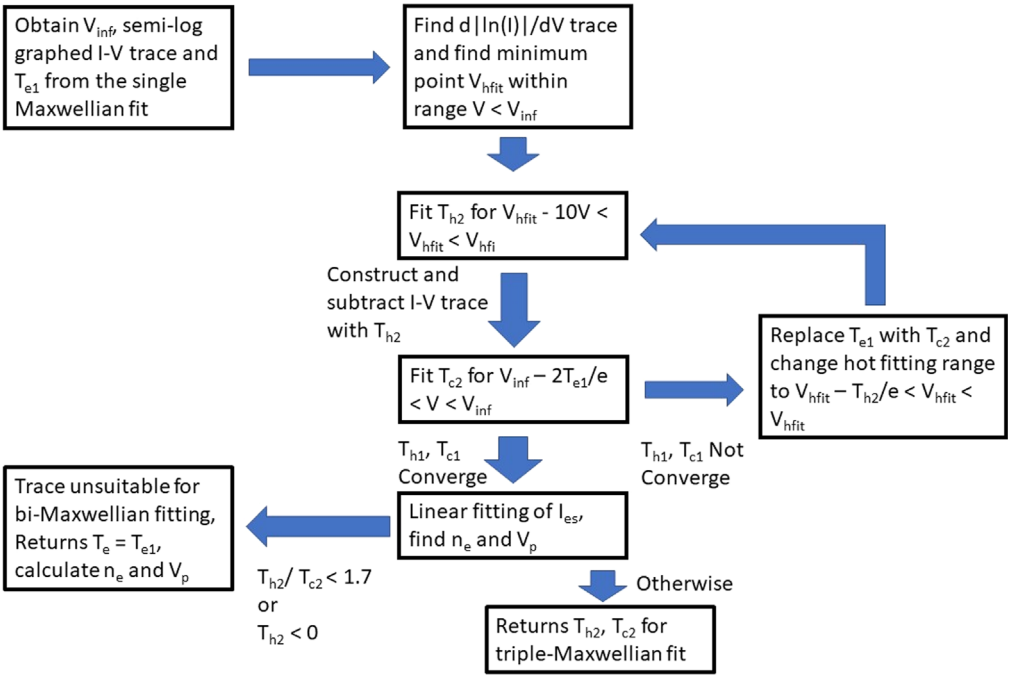


**Figure 5.** Flow chart for the double Maxwellian fitting algorithm.

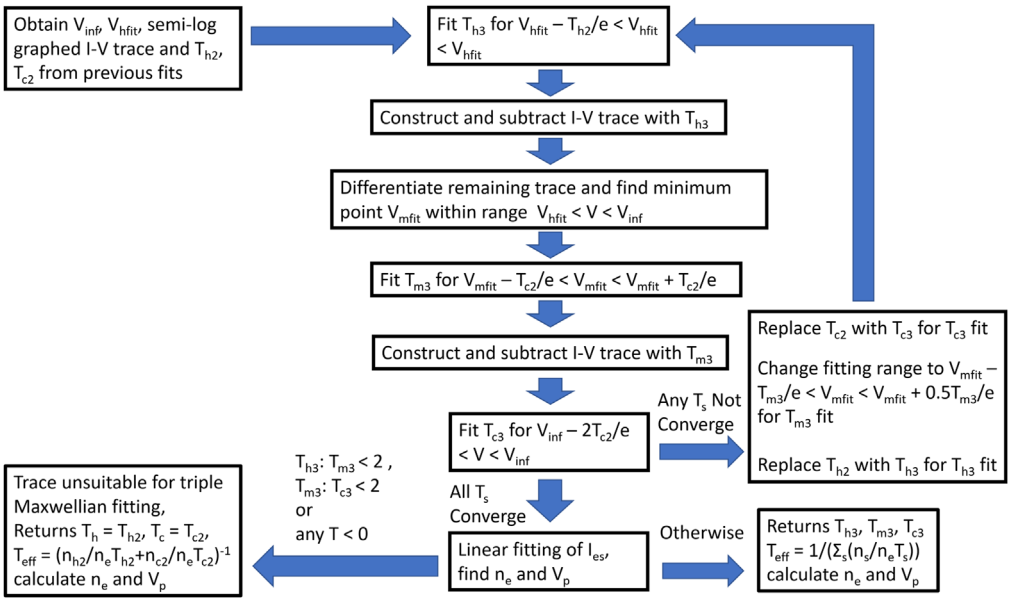


**Figure 6.** Flow chart for the triple Maxwellian fitting algorithm.

subtracted. One should note that for *I*–*V* traces with multiple Maxwellian EEDFs, the contribution from the colder electron population reduces more rapidly than the contribution from the hotter ones as voltage decreases, as a direct result of the Boltzmann relation. This effect favors a fitting procedure of multiple Maxwellian EEDFs that starts with fitting and subtracting the hottest population because the hotter populations can be separated from the colder ones simply by selecting a very negative region on the *I*–*V* trace [24]. To ensure fitting for the hottest population on the *I*–*V* trace, the ln(*I*) is differentiated and the voltage point $V_{\rm hfit}$ with the minimum absolute value of $|{\rm d}(\ln(I))/{\rm d}V|$ is found within the range of $V < V_{\rm inf}$. Then $T_{\rm h2}$ is fitted in the range of $V_{\rm hfit} - 10\,{\rm V} < V < V_{\rm hfit}$. The 10 V fitting range is a seeding value which will be replaced by $T_{\rm h2}/e$ in subsequent iterations, and the choice of $V_{\rm hfit}$ reflects the region of the *I*–*V* trace that can be fitted with the maximum temperature. This avoids a region where a poor signal-to-noise ratio results in the current fluctuating across zero, with the ln(*I*) exploding negatively, corresponding to falsely cold temperatures. A hypothetical *I*–*V* trace is then constructed beyond the inflection point $V_{\rm inf}$ with this fitted $T_{\rm h2}$ to be subtracted from the actual *I*–*V* trace. This range selection and fitting process is illustrated in figure 7(b). Then the temperature of the cold electron population $T_{\rm c2}$ is

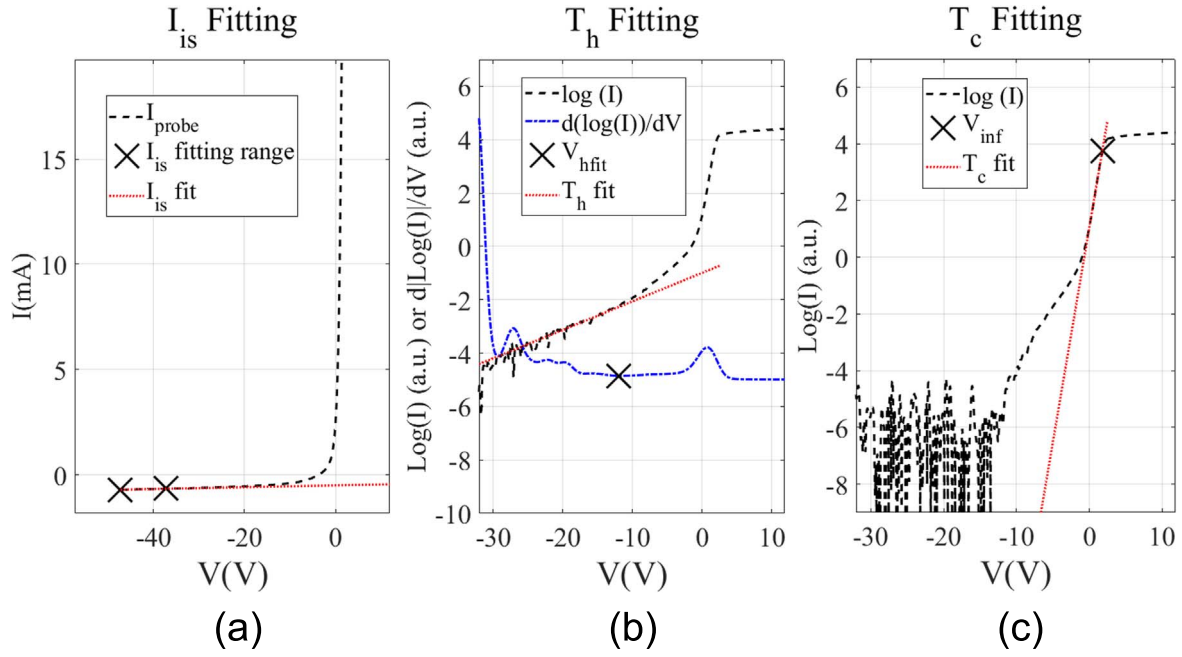


**Figure 7.** Determining the fitting range for $I_{is}$ (a), $T_h$ (b) and $T_c$ (c) after the current contribution from the hot electron population has been subtracted. *I–V* trace is measured in the DTS device with 0.38 Pa argon neutral pressure and discharge current of $I_{Dis} = 0.5$ A. The fitted $I_{is}$, $T_h$ and $T_c$ are reconstructed with the red dotted line.

determined from the remaining *I–V* trace in the fitting range of $V_{inf} - T_{e1}/e < V < V_{inf}$ on a semi-log graph, as illustrated in figure 7(c). The fitting process for $T_{h2}$ and $T_{c2}$ is then re-iterated with the $T_{c2}$ fitting range being $V_{inf} - T_{c2}/e < V < V_{inf}$ and the $T_{h2}$ fitting range being $V_{hfit} - T_{h2}/e < V < V_{hfit}$, until $T_{h2}$ and $T_{c2}$ converge to values within 1%. Several conditions render the *I–V* trace unfit for double Maxwellian fitting and terminate the program, returning $T_e = T_{e1}$: either $T_{h2} < T_{c2}$, or if a negative temperature appears in any iteration, or the final $T_h/T_c < 1.7$. These conditions remove unphysical results and cases where the two temperatures are not sufficiently different such that their fitting ranges might overlap, in which case the *I–V* trace will be best approximated by a single Maxwellian EEDF.

If the fitting process returns valid $T_{h2}$ and $T_{c2}$, a hypothetical trace constructed with both the electron populations will then be drawn to find its intercept with the linearly fitted electron saturation current, from which the density of the cold population $n_{c2}$, that of the hot population $n_{h2}$ and the total density $n_{e2} = n_{c2} + n_{h2}$ will then be calculated.

Plasmas are not always best described by double Maxwellian EEDFs. In some plasmas like multi-dipole confined filament discharges, however, the 'mid-temperature' secondary electrons from the walls are sufficiently different from degraded primaries and plasma electrons produced by ionization so that they forming three electron species plasmas. There is thus a need for an in-depth analysis of their EEDFs [10].

The triple Maxwellian fitting process is similar to the double Maxwellian one, but with an additional step of fitting and subtracting a 'mid-temperature' population from the *I–V* trace between the fitting process of $T_{h2}$ and that of $T_{c2}$. This is done by natural logging and differentiating the *I–V* trace to find a second minimum point $V_{mfit}$ with the range $V_{hfit} < V < V_{inf}$. Then the temperature of the 'mid-temperature' population $T_{m3}$ will be fitted in the range of $V_{mfit} - T_{c2}/e < V < V_{mfit}$ for the first iteration and with the range $V_{mfit} - T_{m3}/e < V < V_{mfit}$ for subsequent ones. This process is illustrated in figure 8. With triple Maxwellians the fitting range of the temperature of the coldest electron species $T_{c3}$ can be extended to $V_{inf} - 2T_{c2}/e < V < V_{inf}$, as subtraction of the hotter species reduces their distortion to the fitting of the coldest one. Fitting is again re-iterated, $T_{h3}$, $T_{m3}$ and $T_{c3}$ replacing $T_{h2}$ and $T_{c2}$ until $T_{h3}$, $T_{m3}$ and $T_{c3}$ converge to 1%. If $T_{h3}/T_{m3} < 1.7$ or $T_{m3}/T_{c3} < 1.7$, or if a negative temperature

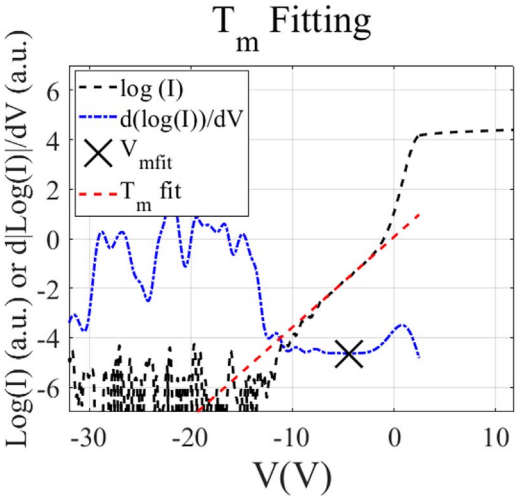


**Figure 8.** Determining the fitting range for $T_m$ for the same *I–V* trace as figure 7, after current contribution from the hot electron population has been subtracted.

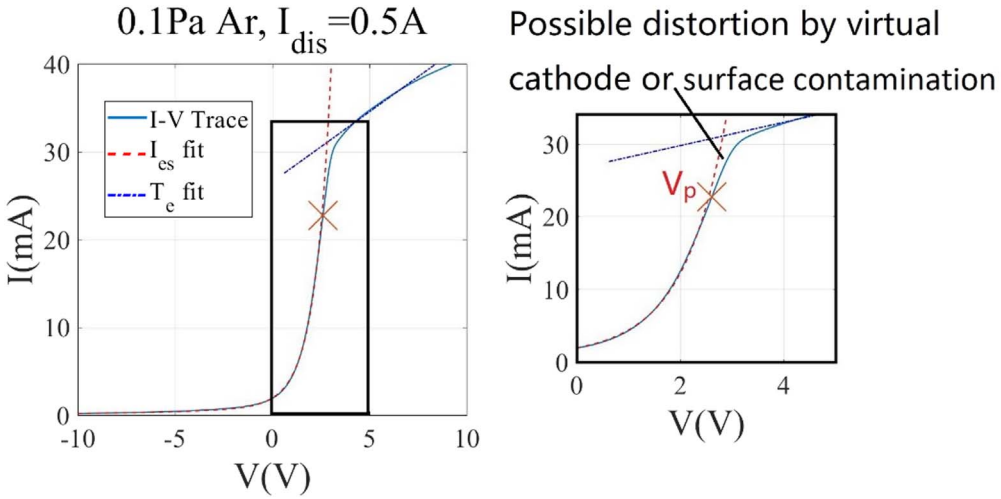


**Figure 9.** A Langmuir probe *I–V* trace (cyan solid line) from the DTS device automatically fit with the triple Maxwellian procedure (red dashed line). In this plasma, measured parameters are $T_{\rm eff} = 0.83$ eV and $n_{\rm e} = 1.2 \times 10^{10}$ cm$^{-3}$.

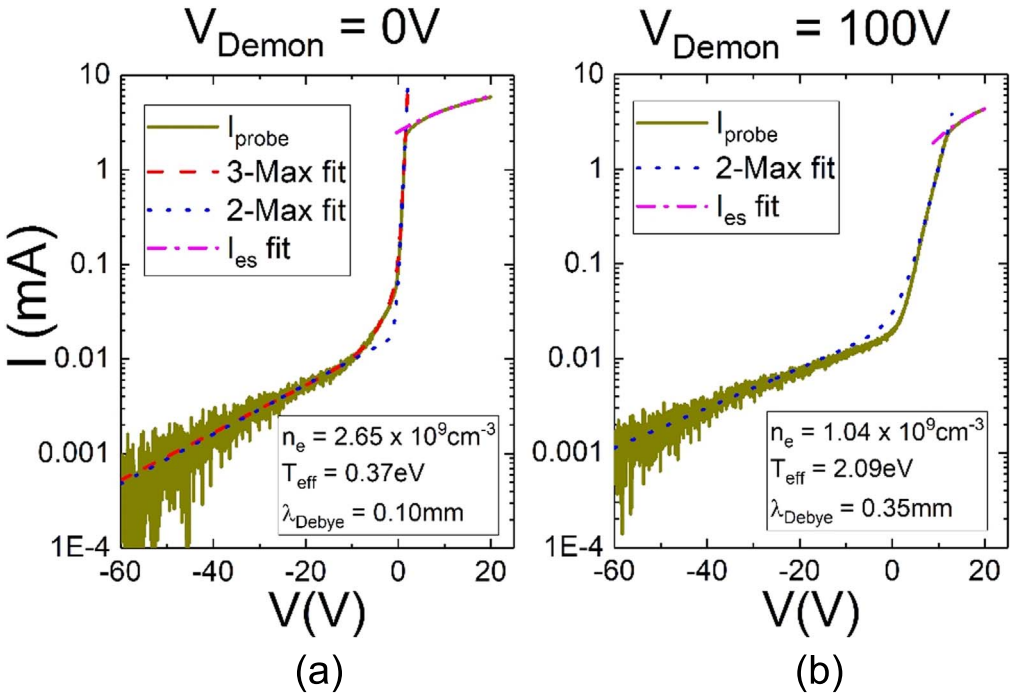


**Figure 10.** Double Maxwellian (2-Max) and triple Maxwellian (3-Max) fitted Langmuir probe traces from the multi-dipole filament discharge at the University of Wisconsin–Madison, with $V_{\rm Demon} = 0$ V (a) and $V_{\rm Demon} = 100$ V (b). Measurements are taken in a 0.4 Pa argon discharge with 0.3 A discharge current.

appears in any iteration, then triple Maxwellian fitting is invalid and the program shall return $T_{\rm eff} = (n_{\rm c2}/(n_{\rm e}T_{\rm c2}) + n_{\rm h2}/(n_{\rm e}T_{\rm h2}))^{-1}$. Otherwise, an *I–V* trace will be constructed with all three electron populations to obtain $I_{\rm es}$ as described above. The effective electron temperature will be given by $T_{\rm eff} = (n_{\rm c3}/(n_{\rm e}T_{\rm c3}) + n_{\rm m3}/(n_{\rm e}T_{\rm m3}) + n_{\rm h3}/(n_{\rm e}T_{\rm h3}))^{-1}$, where $n_{\rm c3}$, $n_{\rm m3}$, $n_{\rm h3}$ are densities calculated by using the current value on their respective hypothetical *I–V* traces at $V_{\rm p}$ and $n_{\rm e} = n_{\rm c3} + n_{\rm m3} + n_{\rm h3}$.

After each fitting process is completed, an *I–V* trace constructed using the parameters from the fitting process will be displayed on both linear and semi-log graphs, along with the measured *I–V* trace for the user to inspect the validity of the automated fitting.

## 4. Experimental results

Figure 9 shows a Langmuir probe trace measured in a DTS discharge at 0.1 Pa argon neutral pressure and 0.5 A discharge current with its ion saturation current subtracted. Reconstruction of the *I–V* trace through automated triple

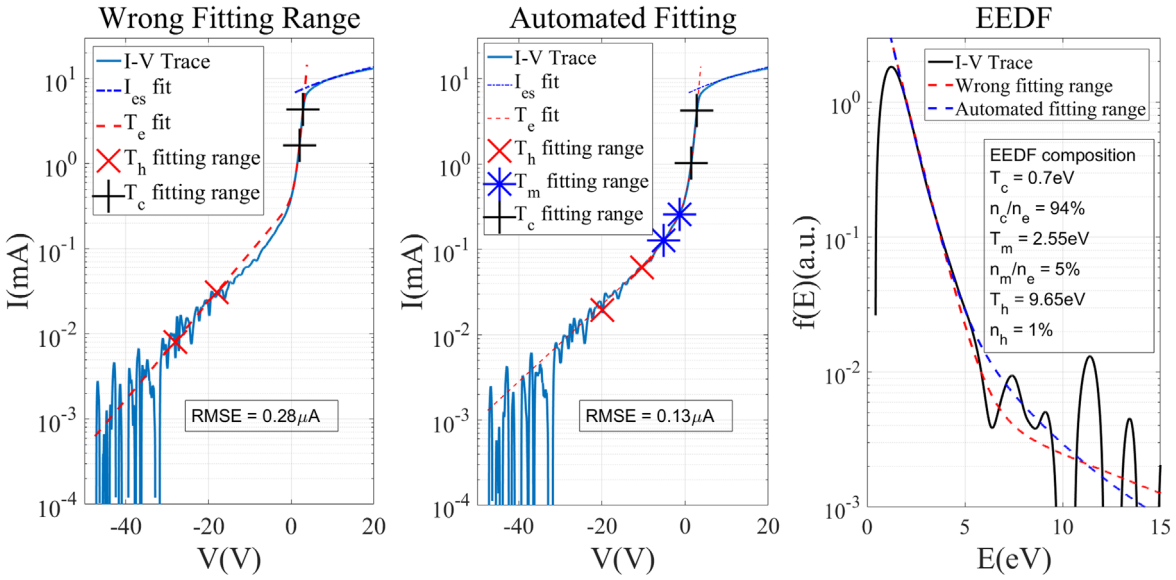


**Figure 11.** *I–V* traces taken in a 0.05 Pa, $I_{\mathrm{Dis}} = 0.2$ A argon discharge in the DTS device fitted with incorrect and correct fitting ranges. Measured parameters are $T_{\mathrm{eff}} = 0.73$ eV, $n_{\mathrm{e}} = 3.2 \times 10^{9}$ cm$^{-3}$ and $\lambda_{\mathrm{Debye}} = 0.13$ mm.

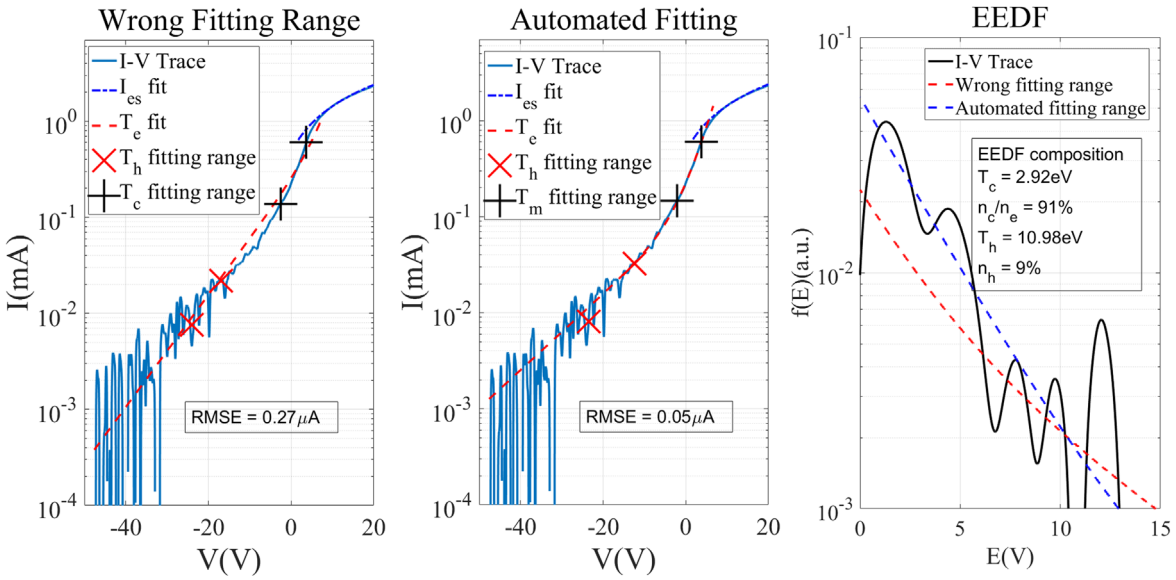


**Figure 12.** *I–V* traces taken in a 0.005 Pa, $I_{\mathrm{Dis}} = 0.2$ A argon discharge in the DTS device fitted with incorrect and correct fitting ranges. Measured parameters are $T_{\mathrm{eff}} = 3.1$ eV, $n_{\mathrm{e}} = 1.8 \times 10^{8}$ cm$^{-3}$ and $\lambda_{\mathrm{Debye}} = 0.93$ mm.

Maxwellian fitting shows good agreement with the *I–V* trace until approximately 0.5 $T_{\mathrm{e}}/e$ near $V_{\mathrm{p}}$. This portion of the *I–V* trace is known to be affected by virtual cathodes and surface contaminations [13–15]. It is unlikely that this relatively slight flattening reflects a real transition to saturation since the current still increases by more than 20% (22.7 mA versus 27.4 mA) within $0.16T_{\mathrm{e}}/e$ before flattening at the characteristic 'knee' of the *I–V* trace of a planar probe. This issue, consistent with previous studies, is the reason why $V_{\mathrm{inf}}$ and $I_{\mathrm{inf}}$ are not immediately selected as the plasma potential and the saturation current respectively. The interception technique and the inflection point can result in an approximately 10% disagreement in $V_{\mathrm{p}}$ (2.61 V versus 2.88 V) but a 40% disagreement in $I_{\mathrm{es}}$ (22.7 mA versus 31.2 mA).

*I–V* traces from the University of Wisconsin–Madison's multi-dipole filament discharge with and without a Maxwell Demon [5, 10] turned on were analyzed using the fitting algorithm to test its effectiveness. When the Demon is turned off, a ~0.4 Pa argon multi-dipole confined filament discharge usually exhibits three Maxwellian electron populations: degraded primary electrons, secondary emitted electrons from the walls, and ionization electrons. With increasing bias on the Demon $V_{\mathrm{Demon}}$, the triple Maxwellian EEDF is eventually reduced to a double Maxwellian EEDF

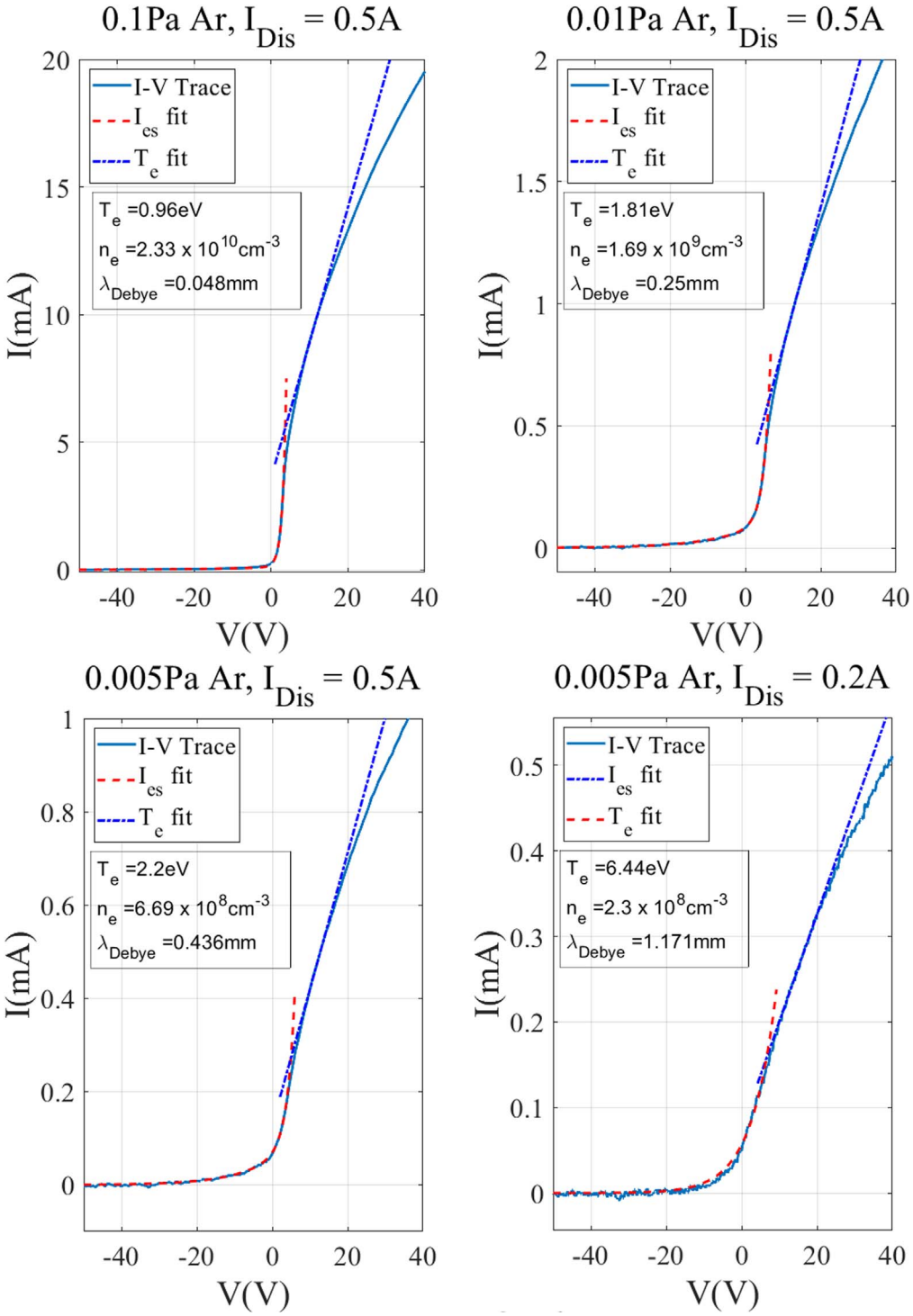


**Figure 13.** *I–V* traces of a cylindrical probe with decreasing neutral pressures and discharge currents.

with only the degraded primaries and a 'cold' population with its temperature at or above that of the secondary electrons from the walls [10, 16]. Figure 10 shows two *I–V* traces, with their ion saturation current subtracted, in such plasma with the $V_{\mathrm{Demon}} = 0\,\mathrm{V}$ and $V_{\mathrm{Demon}} = 100\,\mathrm{V}$. As shown in the figure, the algorithm reconstructed both traces with triple and double Maxwellian EEDFs with good agreement matching both traces. The algorithm also determined that the $V_{\mathrm{Demon}} = 100\,\mathrm{V}$ trace is not suitable for triple Maxwellian fitting as it detected a meaningless negative $T_{c3}$, which is usually due to a lack of significant signal for the fitting process to iterate. It should also be noted that in the $V_{\mathrm{Demon}} = 100\,\mathrm{V}$ case, mid-energy electrons are depleted as the Demon raises the electron

temperature to a point where electrons that form the population's tail are non-existent. This is consistent with previous studies [10, 16].

Figure 11 demonstrates the significance of determining the correct fitting range for both cold and hot electron populations. It shows a planar Langmuir probe trace in a 0.05 Pa, 0.2 A plasma, with its ion saturation current subtracted, that has been deliberately fitted with an incorrect fitting range for the degraded primary electron population and with the automated algorithm. As shown in the figure, fitting the trace with an incorrect fitting range causes the density of the degraded primary electron population to be overestimated, which in turn causes the mid-temperature population to become undetectable. When the signal-to-noise ratio is poor, this effect can be more profound, as shown in figure 12, in which another planar Langmuir probe trace in a 0.005 Pa, 0.2 A plasma is similarly fitted with incorrect and automated fitting ranges. One can see that the reconstructed *I–V* trace severely mismatches the measured *I–V* trace. In these cases, the fitted temperature is not a reliable estimate of $T_e$.

Figure 13 shows a series of *I–V* traces obtained using a 0.15 mm diameter, 19 mm long cylindrical Langmuir probe for various neutral pressures and discharge currents, with their ion saturation currents subtracted to facilitate electron temperature fitting. When the Debye length $\lambda_{Debye}$ is much smaller than the probe's radius $r_{probe}$, the probe behaves as a planar probe even when it is cylindrical, as sheath expansion is small compared to $r_{probe}$. As neutral pressure and discharge current decrease, $n_e$ decreases and thus the Debye length increases. As shown in figure 13, as $\lambda_{Debye}$ becomes much longer than $r_{probe}$, the probe starts to behave as a cylindrical probe. This is signified by the 'knee' of the *I–V* trace becoming less clear as neutral pressure and $I_{Dis}$ decrease. If a significant portion of the noise comes from outside the plasma, reducing $n_e$ also reduces the signal-to-noise ratio as the probe's collected current decreases. This reduction of signal-to-noise ratio can affect cylindrical and spherical probes ($r_{probe} \ll \lambda_{Debye}$) more significantly because their electron saturation currents grow much steeper than that of a planar probe due to sheath expansion effects. This results in increased $dI/dV$ beyond $V_p$ which affects the determination of $V_{inf}$. This is illustrated in figures 13 and 14. Note that in figure 14 the smoothed *I–V* trace, used to produce $dI/dV$, almost overlaps the raw *I–V* trace. In this plasma, $r_{probe}/\lambda_{Debye}$ is between $1/10$ to $1/15$ for the cylindrical probe, which ensures that the probe is sufficiently cylindrical with respect to the plasma. A fitting with a manually selected lower $V_{inf}$, shown in figure 15, is a notably better fitting to the *I–V* trace despite all other fitting parameters still being determined automatically. This also shows why using cylindrical probes is often unfavorable under low signal-to-noise situations. Should cylindrical probes be used in these situations, using an emissive probe to determine the correct $V_p$ will result in much better $T_e$ fitting, but only when global electron flows are absent. Note that one can always obtain a fitted parameter if one smooths the *I–V* trace enough for the fitting algorithm to find a consistent result, but the physical information of the *I–V* trace is gradually lost through smoothing. Thus, the acceptable signal-to-noise ratio is dependent on the degree of error acceptable to the user of the algorithm. The *I–V* trace shown in figures 13(d) and 14 has a noise to electron saturation current ratio of approximately 1:10 before smoothing, which would be close to the minimum acceptable signal-to-noise ratio for the purpose of this work.

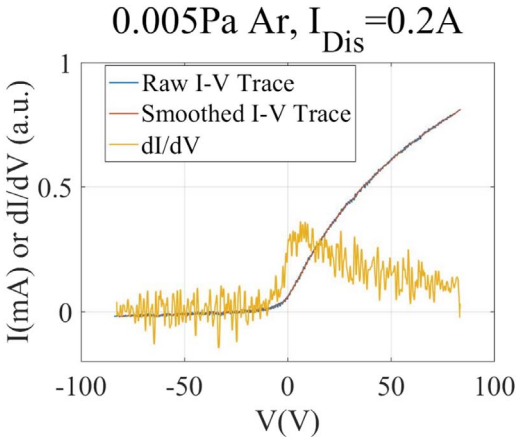


**Figure 14.** A cylindrical probe *I–V* trace and its derivative of a 0.005 Pa, $I_{Dis} = 0.2$ A argon plasma.

Also shown in figure 15 is an automatically analyzed *I–V* trace of a planar probe in a similar discharge. The planar probe is almost immune to the issue of the $V_{inf}$ being unclear as its transition to electron saturation is much more pronounced due to reduced sheath area expansion relative to the probe's area. The planar probe trace also shows a clear double Maxwellian distribution, due to increased signal-to-noise ratio. Note that a probe is physically cylindrical only when $r_{probe} \ll \lambda_{Debye}$, with typical cylindrical probes constructed with 0.15 mm diameter tungsten wires. This means that for plasmas with $n_e > 10^9$ cm$^{-3}$ and $T_e \approx 1$ eV, these probes are unlikely to be affected by the effects portrayed in figure 14 as they physically behave like planar probes, even when they are cylindrical. However, they not directional probes.

## 5. Conclusion

By far the most comprehensive method to analyze a Langmuir probe *I–V* trace is to directly obtain the measured EEDF through the Druyvesteyn method [11]. However, this method requires very good signal-to-noise ratio that might not be available. In these situations, conventional fitting of the *I–V* trace for $T_e$ and $n_e$ is much more practical method as noise amplifications through the associated differential operations are avoided. It should also be noted that even EEDFs extracted through the Druyvesteyn method often need to be fitted for $T_e$ on semi-log graphs in order to be physically understood. In either case, fitting the *I–V* trace reconstructs the measured data through a combination of known distribution forms (in the case of this work, Maxwellian

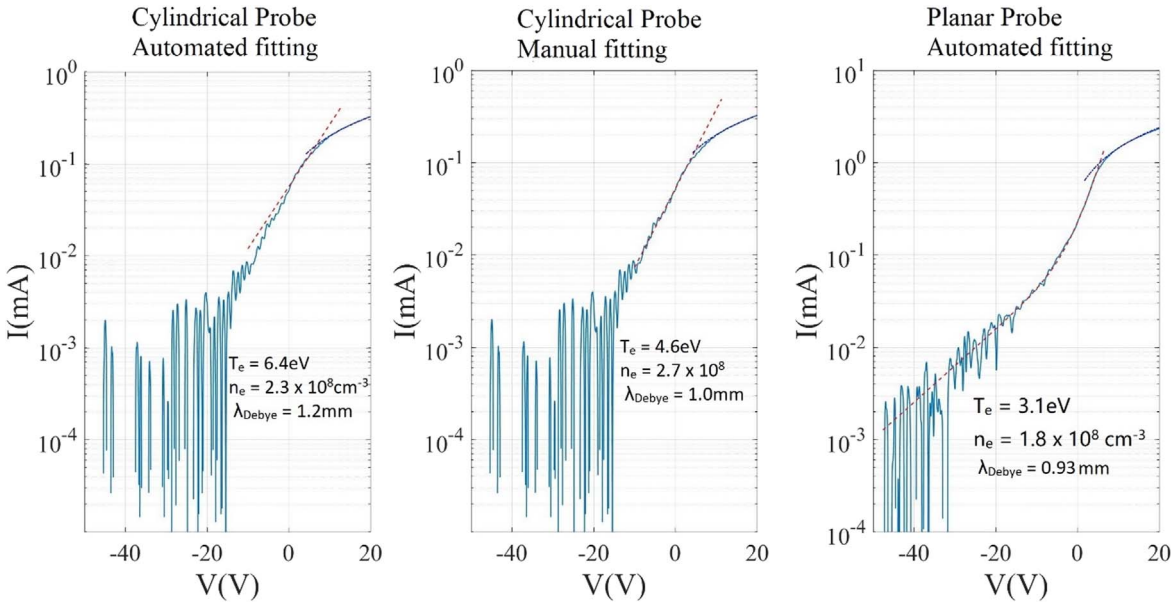


**Figure 15.** A 0.15 mm diameter cylindrical Langmuir probe trace in a 0.005 Pa, $I_{\mathrm{Dis}} = 0.2$ A argon plasma analyzed through automatically and manually selecting $V_{\mathrm{inf}}$. Also included is an automatically analyzed planar probe trace in a discharge with similar neutral pressure and discharge current.

distributions) and finds the parameters that best reproduce the *I–V* trace. For parameters to be accurately extracted, a suitable fitting range must be decided. This is particularly important with multiple Maxwellian fitting in which the fitting range must both satisfy a reasonable signal-to-noise ratio and avoid the portion of the *I–V* trace where contributions of multiple electron populations overlap significantly. This is the primary reason why, if needed, multiple Maxwellian fittings have often been fitted manually in previous studies [10, 16]. However, for experiments that have very large amount of data, fitting *I–V* traces manually is unrealistic. In this work, we present an iterative algorithm to automatically choose the fitting range for each electron temperature population, so that the position and size of the fitting range traces the temperature of the corresponding electron population, providing physically valid fitting ranges. The algorithm also fits the *I–V* trace for the plasma potential, provided that the EEDF is not drifting. The algorithm also defines criteria for which an *I–V* trace is not suitable for double or triple Maxwellian fitting and returns results of the lower order fittings if such criteria are satisfied. This is also important because, as experimental data show, not all EEDFs in all plasma sources under different working conditions can be properly described by single, double or triple Maxwellian distributions. These criteria act as fail-safe measures to prevent the automated procedures returning unphysical results under these circumstances.

It is also found that for probes behaving physically cylindrically as the Debye length increases with decreasing plasma density, poor signal-to-noise ratio significantly affects the determination of $V_{\mathrm{inf}}$. This is because cylindrical sheath expansion results in higher $\mathrm{d}I/\mathrm{d}V$ beyond $V_{\mathrm{p}}$. This in turn affects the determination of $V_{\mathrm{inf}}$ and the fitting range for $T_{\mathrm{e}}$, as well as the plasma potential. In these cases, planar probes are recommended due to their pronounced transition to saturation resulting in a clear $V_{\mathrm{inf}}$.

## Acknowledgments

This work is supported by the Chinese Academy of Science Hundred Youth Talent Program Start-up Funding, CAS Key Research Program of Frontier Sciences (No. QYZDB-SSW-SLH001), National Natural Science Foundation of China (Nos. 11875285, 11575248 and 11505220), as well as US National Science Foundation Award (No. 1804654).

## References

[1] Langmuir I 1925 *Phys. Rev.* **26** 585
[2] Xu J C *et al* 2018 *IEEE Trans. Plasma Sci.* **46** 1331
[3] Xu J C *et al* 2016 *Rev. Sci. Instrum.* **87** 083504
[4] Bilik N *et al* 2015 *J. Phys. D: Appl. Phys.* **48** 105204
[5] MacKenzie K R *et al* 1971 *Appl. Phys. Lett.* **18** 529
[6] Itagaki N *et al* 2001 *Thin Solid Films* **390** 202
[7] Cao X G *et al* 2015 *Plasma Sci. Technol.* **17** 20
[8] Mendil D, Lahmar H and Boufendi L 2014 *Plasma Sci. Technol.* **16** 837
[9] Barnat E V and Weatherford B R 2015 *Plasma Sources Sci. Technol.* **24** 055024
[10] Yip C S *et al* 2013 *Plasma Sources Sci. Technol.* **22** 065002
[11] Godyak V A and Demidov V I 2011 *J. Phys. D: Appl. Phys.* **44** 233001
[12] Popov T K *et al* 2012 *Plasma Sources Sci. Technol.* **21** 025004
[13] Yip C S and Hershkowitz N 2015 *J. Phys. D: Appl. Phys.* **48** 395201
[14] Stamate E and Ohe K 2002 *J. Vac. Sci. Technol.* A **20** 661
[15] Thomas T L and Battle E L 1970 *J. Appl. Phys.* **41** 3428

[16] Yip C S and Hershkowitz N 2015 *Plasma Sources Sci. Technol.* **24** 034004
[17] Mizumura M *et al* 1992 *J. Phys. D: Appl. Phys.* **25** 1744
[18] Limpaecher R and MacKenzie K R 1973 *Rev. Sci. Instrum.* **44** 726
[19] Riemann K U 1991 *J. Phys. D: Appl. Phys.* **24** 493
[20] Riemann K U 1995 *IEEE Trans. Plasma Sci.* **23** 709
[21] Hershkowitz N 1989 How langmuir probes work ed O Auciello and D L Flamm *Plasma Diagnostics* (New York: Academic)
[22] Sheridan T E 2000 *Phys. Plasmas* **7** 3084
[23] Lee D and Hershkowitz N 2007 *Phys. Plasmas* **14** 033507
[24] Godyak V A, Piejak R B and Alexandrovich B M 1993 *J. Appl. Phys.* **73** 3657